NASA Technical Memorandum 110407

A Thermostructural Analysis of a Diboride Composite Leading Edge

Tom Kowalski, Kent Buesking, Paul Kolodziej, and Jeff Bull

July 1996

National Aeronautics and
Space Administration

NASA Technical Memorandum 110407

A Thermostructural Analysis of a Diboride Composite Leading Edge

Tom Kowalski, Eloret Thermosciences Institute, Palo Alto, California
Kent Buesking, MSNW, Inc., San Marcos, California
Paul Kolodziej and Jeff Bull, Ames Research Center, Moffett Field, California

July 1996

National Aeronautics and
Space Administration

Ames Research Center
Moffett Field, California 94035-1000

A Thermostructural Analysis of a Diboride Composite Leading Edge

TOM KOWALSKI,* KENT BUESKING,† PAUL KOLODZIEJ, AND JEFF BULL

Ames Research Center

Summary

In an effort to support the design of zirconium diboride composite leading edges for hypersonic vehicles, a finite element model (FEM) of a prototype leading edge was created and finite element analysis (FEA) was employed to assess its thermal and structural response to aerothermal boundary conditions. Unidirectional material properties for the structural components of the leading edge, a continuous fiber reinforced diboride composite, were computed with COSTAR. These properties agree well with those experimentally measured. To verify the analytical approach taken with COSMOS/M, an independent FEA of one of the leading edge assembly components was also done with COSTAR. Good agreement was obtained between the two codes. Both showed that a unidirectional lay-up had the best margin of safety for a simple loading case. Both located the maximum stress in the same region and ply. The magnitudes agreed within 4 percent. Trajectory based aerothermal heating was then applied to the leading edge assembly FEM created with COSMOS/M to determine steady state temperature response, displacement, stresses, and contact forces due to thermal expansion and thermal strains. Results show that the leading edge stagnation line temperature reached 4700°F. The maximum computed failure index for the laminated composite components peaks at 4.2, and is located at the bolt flange in layer 2 of the side bracket. The temperature gradient in the tip causes a compressive stress of 279 ksi along its width and substantial tensile stresses within its depth.

Nomenclature

C_h	heat transfer coefficient
C_p	specific heat at constant pressure
h	enthalpy, J/kg
q	heat flux, W/m^2
q_{rad}	radiant heat flux, W/m^2
S_{12}^+	positive in plane shear strength in the material x-y plane
S_{12}^-	negative in plane shear strength in the material x-y plane
T	temperature, K
X_1^C	compressive strength in the material longitudinal direction
X_1^T	tensile strength in the material longitudinal direction
X_2^C	compressive strength in the material transverse direction
X_2^T	tensile strength in the material transverse direction
σ_1	first principal stress
σ_2	second principal stress
τ_{12}	shear stress in x-y plane

Subscripts

r	recovery
s	symmetric
w	wall
0	stagnation conditions

Introduction and Approach

The present space shuttle design is limited in performance by the relatively low lift-to-drag (L/D) ratio of its airfoils. Its leading edge and nose cap are constrained to blunt geometries so that operational temperatures will not cause excessive material degradation or ablation in multiple reuse. Materials with higher temperature capability and greater ablation resistance will allow spacecraft designers to develop airfoils with sharper leading edge radii, higher L/D ratios, and better performance.

Ultra-high temperature ceramic (UHTC) materials are being investigated for leading edge applications in advanced airframes at Ames Research Center (ref. 1). These materials have been evaluated in the Ames arc-jet test facilities, which can reproduce flow conditions

*Eloret Thermosciences Institute, Palo Alto, California.
†MSNW, Inc., San Marcos, California.

representative of hypersonic flight. A prototype leading edge assembly is shown in figure 1. It was designed to demonstrate, quickly and simply, the functional performance of a sharp leading edge using existing UHTC materials. It is specifically designed for testing in an arc jet, although its size and configuration may be directly applicable to hypersonic vehicles. An exploded view of the assembly is shown in figure 2. The illustration shows two UHTC tip inserts, components 3 and 4. In the arc-jet test, or on a hypersonic vehicle, it is highly desirable to secure the tip inserts with a hot structure rather than an actively cooled one. A passively cooled attachment will prevent severe thermal gradients in the tip material, significantly reduce thermal protection system (TPS) weight and complexity, and increase its reliability and durability. Therefore, the four brackets, components 1, 2, 5, and 6, are fabricated from a continuous fiber reinforced UHTC composite. Although still in development, this material is designed to be a load bearing hot structural material which is both thermochemically and thermomechanically compatible with the tip material. The arc-jet facility attachment, component 7, is a metallic structural attachment for the arc-jet facility sting.

Initially, it was assumed that the top and bottom brackets, components 5 and 6 in figure 2, were the most vulnerable of all the components in the assembly since expansion of the tip inserts will force the brackets outward and, because of the bolted constraints, will create bending stresses at the root. Accordingly, the top bracket was modeled with the finite element method using COSTAR and COSMOS/M finite element analysis (FEA) codes. COSTAR is particularly well suited for the analysis of structures which incorporate composite materials but is not versatile enough to handle large multicomponent assemblies. Additionally, FEA using COSTAR with similar ceramic matrix composites (CMC) has been demonstrated (ref. 2). The COSTAR analysis was completed under contract by MSNW, Inc., San Marcos, California, and is reported in reference 3. The reason for the duplicate analysis was to lend credibility to our COSMOS/M analysis with composite materials, which had not been done previously.

The fiber volume fraction and fiber orientations of the bracket material were important considerations to ensure that the brackets had adequate structural integrity to survive the severe heating environment. Several orientations and fiber loading were evaluated using COSTAR, and directional material properties were calculated. Iterations on these calculations were made until reasonable agreement was obtained with experimentally measured values. These properties were then used in both COSTAR and COSMOS/M for FEA. The results of these two independent analyses performed on the top brackets were compared and noted before proceeding with FEA of the leading edge assembly.

For each structural analysis of layered composites presented in this report, stress results are presented in terms of Tsai-Wu failure criteria. Similar to a safety factor, the Tsai-Wu criteria (F.I.) are a function of principal stresses and ultimate strengths of the material. The Tsai-Wu criteria used here are defined by equation (1).

$$\text{F.I.} = \left(F_1\sigma_1 + F_2\sigma_2 + F_6\tau_{12}\right) + \left(F_{11}\sigma_1^2 + F_{22}\sigma_2^2 + F_{12}\sigma_1\sigma_2 + F_{66}\tau_{12}^2\right) \quad (1)$$

where

$$F_1 = \frac{1}{X_1^T} - \frac{1}{X_1^C}, \quad F_2 = \frac{1}{X_2^T} - \frac{1}{X_2^C},$$

$$F_6 = \frac{1}{S_{12}^+} - \frac{1}{S_{12}^-}, \quad F_{11} = \frac{1}{X_1^T X_1^C},$$

$$F_{22} = \frac{1}{X_2^T X_2^C}, \quad F_1 = \frac{1}{S_{12}^+ S_{12}^-}, \quad F_{12} = 0$$

A value of 1.0 denotes the onset of failure. These criteria were calculated for each layer in the composite. The highest values tend to be in the outer two layers of the composite.

Modeling and analyzing the entire leading edge assembly serves to pinpoint the exact areas of contact governed by the interaction of all components within it as it is thermally loaded and also identifies locations and magnitudes of thermally induced stresses in each of the components. But it is the contact loads that determine the structural integrity of the attachment concept. With this information one can assess whether the materials and design are compatible and the design concept is thermostructurally viable. This type of analytical approach will be instrumental in future designs of similar TPS.

The assumptions regarding the boundary conditions used in the COSMOS/M and COSTAR analyses of the top bracket, region of contact and local temperature, were later refined in modeling the leading edge assembly. A trajectory based aerothermal boundary condition was obtained by selecting a coordinate on the tip material's aerothermal performance constraint which coincided with conditions obtainable in ground test facilities (arc jets) and with a coordinate on a projected hypersonic vehicle's flight trajectory (ref. 4). From this initial condition, boundary conditions were calculated as a function of

streamline distance so that the heating distribution over the entire assembly could be properly treated.

Analyses and Results

Composite Materials and Properties

In order to properly design the leading edge, it is necessary to understand the material behavior and compute accurate stresses in its components caused by the operating conditions. The objectives in analyzing the composite material behavior are to (1) develop a realistic micromechanical model of the composite material properties, (2) compute properties for composites made with various fiber volume fractions, (3) select an optimized laminate design for fabrication and testing.

The tip inserts, components 3 and 4 in figure 2, are fabricated from a ZrB_2/SiC particulate composite with SiC as the minor phase. Billets of this material are processed by unidirectional hot-pressing and the inserts are machined from the center of a billet. Material properties for ZrB_2/SiC were obtained from the Ames TPSX database and were assumed to be isotropic for these analyses. Processing of the ZrB_2/SiC material has been refined by White Materials Engineering of Cumberland, Rhode Island, under NASA ARC Contract No. NAS2-14242 and is being marketed under the trade name "Zirstar."

The brackets, components 1, 2, 5, and 6 in figure 2, are fabricated from a continuous fiber reinforced diboride particulate composite. The bracket material matrix is of the same composition as the tip inserts but is reinforced with continuous SiC fibers (Textron SCS-9a). It is processed in thin sheets, or lamina, which are then stacked in the direction of choice and consolidated by hot-pressing. The material has been developed by Advanced Ceramics Research of Tucson, Arizona, under NASA ARC Contract No. NAS2-13796. It is designated as SCS9/RBSiC/ZrB_2.

Unidirectional lay-ups, 0° fiber orientation, containing 20.7 vol.% fiber had been characterized extensively in both the fiber and transverse direction. The anisotropic properties of this material were calculated with COSTAR. The calculated modulus of elasticity was adjusted until it agreed reasonably well with that measured over a temperature range from room temperature to 3000°F. The computations resulted in effective mechanical properties of the matrix that were significantly less than those reported for the fully dense ZrB_2/SiC material. One reason for this is because the matrix is heavily microcracked due to the thermomechanical mismatch between the fiber and matrix. Because experimental measurements of the thermal properties were not available, those of ZrB_2/SiC were used. Once agreement was obtained with the 20.7 vol.% loading, the same effective matrix was used in calculating properties for composites with fiber volume fractions of 10, 22.5, and 35 vol.%. It was found that the 0° modulus and tensile strength are linearly dependent on fiber volume fraction, so the composite with 35 vol.% loading exhibits the highest strength. The engineering properties of this material are given in table 1. Because the 35 vol.% loading has the greatest strength, it was chosen for the top bracket bending analysis.

Top Bracket Bending

A finite element model of the leading edge top bracket was developed using COSTAR and COSMOS/M to analyze the performance of 35 vol.% SCS9/RBSiC/ZrB_2 laminates with orientations of 0°, 0°/90°, and 0°/±45°/90°. The models were clamped at the bolt and loaded by a tip deflection that was representative of the thermal growth of the Zirstar leading edge test specimen. All analyses were performed at a uniform temperature of 3000°F. These finite element models were verified by comparison with beam theory calculations.

COSTAR results include the distribution of plate forces and moments within the bracket and ply-level stresses within the composite laminate. Results of the stress analysis showed that the bracket is loaded primarily by a bending moment, which generates longitudinal bending stresses in the bracket. The comparison of the results for the various orientations showed that the unidirectional design (i.e., 0°) exhibited the largest margin of safety of all the laminates that were analyzed. The results also showed that the performance of the 0/90 design was optimized by concentrating the 0° plies at the outside surface of the bracket and situating the 90° plies near the neutral axis. Based on these results, the 0° laminate was selected as the most attractive material design and is recommended for the bracket fabrication.

The COSMOS/M finite element model was created using the same top bracket geometry and material properties as the COSTAR model (see fig. 3 and table 1). The COSMOS model consisted of 890 quadrilateral composite shell elements as did the COSTAR model. The grid included half of the width of the bracket with symmetry conditions (UY = RX = RZ = 0) applied along the centerline. Figure 4 shows the COSMOS/M model mesh. The element coordinate system definition used for stress computation is also described in figure 4. The element coordinate system was chosen such that it matches the coordinate system of the COSTAR model and the coordinate system defined in the geometry description

(fig. 3). The element coordinate system can be visualized as a weave of fibers such that the longitudinal fibers (90° orientation or x direction) always follow the curved profile along the length of the bracket. Nodes at the bolt location were constrained in all three translational degrees of freedom (UX = UY = UZ = 0).

The results for the 0/90 configuration for the outer two plies are shown in the form of Tsai-Wu failure criteria in figures 5–8. Both codes give similar results for stress magnitude and distribution. The highest stress in both models occurs in ply 2 at the bolt interface (see figs. 5 and 8) where the failure index reaches 2.15 for COSTAR and 2.23 for COSMOS. These results suggest that failure will occur in the bolt region of the top bracket when the Zirstar tip expands and bends the bracket. It should be noted that in both models the maximum stresses are unrealistically high due to the constraints imposed to simulate bolting the bracket (constrained in all degrees of freedom). For comparison, the stress for F.I. maximum is plotted in figure 9 for each ply through the thickness. Both codes produce nearly identical results from the outermost ply to the neutral axis for plies 1 and 2. Both codes also produced erratic results after the neutral axis for the 90° plies. The reason for this behavior is not known at this time. Broader contact forces and friction were not considered in this study but would represent a more realistic treatment of the bolt interface for fastening the structure. A detailed, more complex analysis of the bolt region deserves further study.

To refine and validate some of the assumptions used in the COSMOS/M and COSTAR top bracket models, a bi-planar symmetric 3-D thermostructural model of the entire test fixture with trajectory based aerothermal heating was created with COSMOS/M. Benefits of modeling the entire assembly include a more refined temperature distribution that takes into account realistic thermal loading, edge effects due to reradiation, and a better understanding of the component contact locations and contact forces. Although it was found from the top bracket bending analysis that concentrating the 0° plies at the outside surface of the bracket and situating the 90° plies near the neutral axis is preferable for reducing stress in the top bracket, a 0°/90° symmetrical lay-up was used to formulate the full assembly analysis. This is because the model being tested in the arc-jet facility was fabricated with a 0°/90° symmetrical lay-up before the analysis was complete. A major reason for performing a 3-D assembly analysis was to predict the survivability of the leading edge model. However, future prototypes (and analyses) will utilize a 0°/0° lay-up for the outer plies.

Thermal and Structural Analysis of the Leading Edge Assembly

Before the structural response of the leading edge assembly can be determined, an accurate steady state temperature distribution must be established for the condition of interest. To accomplish this, a finite element model (FEM) of the leading edge assembly was created, and heat flux was applied to the exposed surfaces corresponding to a point on an aerothermal performance constraint. Heat flux was applied to the model by prescribing a convection coefficient to each element along the streamline from the stagnation line to the sting mount.

Thermal and structural FEM– To create the FEM used for both the thermal and structural analyses, symmetrical representations of the top and side brackets and tip inserts were meshed with appropriate elements. Geometrical and load symmetry permitted the use of symmetrical constraints about the xy and zx planes to make efficient use of the element density. The mesh assembly is shown in figure 10. A total of 5000 elements were used. The tip insert was modeled with eight node isotropic solid elements. An increased element density was used in the tip region where a high thermal gradient is expected. The top and side brackets were modeled with eight node orthotropic SHELL4L elements. The SHELL4L elements were assigned both thermal and structural orthotropic material properties with temperature dependence. A 20 layer $[0/90]_S$ composite architecture was defined in the SHELL4L real constant set. Material properties were computed for this architecture in the same fashion as that done for the top bracket analysis of this report. Gap elements were used between components to simulate a finite gap on the order of 0.001 inch. As the components expand when heated, and the gap distance becomes zero within a specified tolerance, the components will be capable of reacting together structurally. Unfortunately, gap elements available in COSMOS/M do not have the capability to conduct heat across the gap even if the gap distance becomes zero. In reality, heat conduction will occur when the gap distance approaches zero. To work around this problem, very soft (E_X = 1E-5 psi) TRUSS3D elements with large cross-sectional areas (Acs = 1 in.) and a high thermal conductivity (k_X = 1E5 Btu/h-ft-°F), were positioned coincident with the gap elements to simulate heat conduction between them. The use of the soft conductor bars imposes a constant contact condition without altering structural response.

Boundary conditions– The aerothermal heating conditions were obtained by selecting a coordinate on the tip material's aerothermal performance constraint which coincides with conditions obtainable in ground test facilities (arc jets) and with a coordinate on a projected

vehicle's flight trajectory (ref. 4). Aerothermal performance constraints are computed by taking into account all the various modes of heat dissipation available to a material including reradiation, convective blocking, catalytic effects, and multidimensional conduction (ref. 5). The computation is done assuming steady state heat transfer and results in a material based performance map in altitude-velocity space.

In order to accurately calculate steady state aerothermal performance constraints for UHTC sharp leading edges, it is necessary to analyze the thermal conduction of heat away from the stagnation region. Rather than developing custom thermal analysis software, it is advantageous to use commercially available FEA software tools (COSMOS/M) which are capable of thermal/structural analysis. Because these commercial FEA tools have been developed for application to a wide variety of generic heat transfer problems, there are standard procedures for constructing the model geometry, specifying the element type, and assigning material properties. However, because of the unique characteristics of heat transfer to a nose tip (3-D) or wing (2-D) leading edge in hypervelocity flight, there are no standard procedures for assigning the thermal boundary conditions to the FEA model. It is necessary to develop a custom procedure for assigning the appropriate aerothermodynamic heating boundary condition.

Aerothermodynamic heating of a leading edge in hypervelocity flight has a maximum where the fluid is stagnated, then decreases rapidly as the fluid accelerates downstream. The dependence of this heating distribution on freestream velocity, geometry, fluid properties, and wall temperature was first analyzed by Lee (ref. 6) for simple 3-D and 2-D leading edges. More generalized expressions which are useful for examining complex geometries were developed by Marvin (ref. 7). Both of these approaches provide estimates of normalized heat flux as a function of surface distance from the stagnation point. For a given velocity, geometry, and fluid this distribution simplifies to

$$\frac{q_w}{q_{w,0}} = \frac{C_h(h_r - h_w)}{C_{h,0}(h_r - h_w)_0} \tag{2}$$

Using $h = C_p T$

$$\frac{q_w}{q_{w,0}} = \frac{C_h C_p(T_r - T_w)}{C_{h,0} C_{p,0}(T_r - T_w)_0} \tag{3}$$

If C_p and T_r are constant, then aerothermodynamic heating of a leading edge is given by

$$\frac{q_w}{q_{w,0}} = \frac{C_h(T_r - T_w)}{C_{h,0}(T_r - T_w)_0} \tag{4}$$

where C_h and T_w are functions of surface distance from the stagnation point. Typically, the standard procedure in thermal FEA uses up to four types of boundary conditions (BC) for specifying the thermal load on the model

1. Temperature (T_w)
2. Convection (C_h, T_r)
3. Heat Flux (q_w)
4. Radiation (q_{rad})

With these four alternatives, there are two approaches to specifying aerothermodynamic heating for thermal FEA. In one approach, using BC-2, the heating can be expressed from equation (4) by specifying C_h and T_w as a function of distance along with the constants $q_{w,0}$ and T_r. In the other approach, using BC-3, the heating is expressed from equation (4) by specifying q_w as a function of distance along with the constant $q_{w,0}$. In addition to either approach, BC-2 or BC-3, reradiation must be specified by assigning the appropriate surface emissivity using BC-4.

For the analysis discussed in this study the aerothermodynamic heating $q_w/q_{w,0}$ is specified using the aerothermal performance constraint code PERFORM (ref. 5). Because of the nonlinear coupling between the convective heat transfer from the fluid and the surface temperature of the material due to the reradiation, several iterations are required between PERFORM and COSMOS/M. Convergence on surface temperature usually occurs in less than four iterations when using the BC-2 approach. Convergence is much worse when using the BC-3 approach, and does not occur under some conditions.

The applicable aerothermal performance curve is shown in figure 11(a) along with the position of the selected coordinate, an altitude of 197 kft and a velocity of 29 kft/s. From this coordinate, heat transfer coefficients were computed as a function of streamline distance as shown in figures 11(b) and 11(c). These "hot wall" coefficients were input into COSMOS/M as the boundary conditions representing aerodynamic heating over the entire assembly.

Other necessary thermal boundary conditions include those at the back wall or bolt interface. A constant temperature of 300°F was selected here for several reasons. The heat transfer coefficients computed for this case are nearly the same for an adiabatic back wall case; in both flight and arc-jet testing the assembly is attached to a structure which acts as a large heat sink, and 300°F is a nominal use temperature for many aerospace structures (i.e., carbon/epoxy composites or metallic alloys). An emittance of 0.7 rather than 0.6 was used in the

COSMOS/M analysis for all components because this is the materials database value for the unoxidized surface at the temperature of interest. An emittance of 0.6 is characteristic of the oxidized surface. Using 0.7 results in a lowering of the stagnation line temperature by approximately 300°F from its design limit. The ambient temperature for the COSMOS/M analysis was assumed to be 500°F.

The most critical structural boundary condition is the treatment of the assembly connections. The side and top brackets were considered to be securely bolted to the sting by constraining nodes associated with the fastener boundaries. It is believed to be a conservative approach since some slipping will occur at the bearing surface between the bolt head and the sting. The temperature profile generated from the thermal analysis and associated thermal strains is the sole source of the loads applied to the components of the assembly. The thermal strains are induced by temperature differential and mechanical constraints that restrict thermal growth.

A script utilizing the COSMOS/M command language was developed to map discretized points from a curve fit of s/r versus heat transfer coefficient data onto the leading edge assembly. The script can be applied to any FEA model generated with COSMOS/M by substituting the geometry profile equations, reassigning the element step size and identifying the new stagnation location. (Documentation is embedded in the script which can be found in the Appendix.)

Thermal–Figure 12 shows the steady state temperature distribution at the prescribed aerothermal condition looking from the top-side view. The peak temperature is at the stagnation line of the tip inserts and has a value of 4670°F. The temperature contour lines drifting forward at the model edge are an effect of reradiation conditions imposed at the outward facing surfaces of the top bracket and conduction in the top and bottom brackets, which are twice as thick as the side brackets. The other side of the bracket is not exposed to air, but is in thermal contact with the adjacent leading edge segment.

Structural– Thermal strains develop in components of the assembly from thermal gradients and from mechanically restricting thermal growth. For the top and side brackets, mechanically constraining the thermal growth is the primary contribution to the stresses developed. The bulk of the stress in the tip insert is primarily induced from severe thermal gradients. A major assumption in the preliminary top bracket analysis was that the top bracket is loaded solely by the thermal growth of the tip insert in the z direction. Modeling all components shows that the tip insert imparts very little load to the top bracket. Inspection of the displacement plot in figure 13 (a bottom-side view) reveals that the area of contact is at the rear of the assembly between the side and top/bottom brackets. The gap elements in this region are closed and generate a total compressive force of 383 lbf. This force is listed with other contact forces in table 2. Loading in this region creates a prying effect that causes the tip of the top bracket to separate slightly from the tip insert. The gap created from this separation is predicted to be on the order of 5 mils.

The load built up in the contact region reflects the rigid constraints imposed to simulate the bolted connection. As a result, stresses in the bolt bearing area are extreme. A Tsai-Wu failure index of 4.1 was computed at the bolt region (identified by label L4) in layer 2 of the side bracket as shown in figure 14. If the bolt constraints were realistic, failure would occur in both layers at the bolt interfaces.

Table 3 summarizes the critical stress areas in the loaded bracket (L1–L6). The Tsai-Wu failure indices for ply 1 are shown in figure 14. Critical stress areas for ply 1 include the top bracket's bolted region (L3) and the large bend radius of the top bracket (L1). The stress computed at the large bend radius approaches the material's failure limit and is not considered to be conservative.

Due to severe thermal gradients in the tip insert, considerable tensile and compressive stresses develop. Figures 15 and 16 show a stress contour plot for the z direction for layers 1 and 2, respectively. Because the tip inserts are considered to be made of an isotropic material the results do not vary by layer. Layer results apply only to the top and side brackets. The greatest stresses developed in the leading edge tip insert are compressive with a maximum magnitude of 297 ksi. The location of this stress is shown by the designation L5 in figure 17. The center area of the tip inserts is in tension with a maximum magnitude of 45 ksi. The strength of the zirconium diboride composite is 50 and 500 ksi in flexure and compression, respectively, so the tensile stresses in the tip insert, as shown here, could lead to failure.

Discussion

The static solution indicates that when the model is thermally loaded the contact forces developed between the side and top brackets, as a result of the thermal growth of the top brackets, cause the side brackets to separate from the tip insert. Upon separation, conduction can no longer occur. Therefore, the use of truss elements, while necessary to provide a conduction path across the gap elements, cannot fully simulate the real situation. The inability to capture conduction termination upon separation is a limitation of the FEA code used. If the degree of

thermal conductivity could be defined for each truss element as a function of relative nodal positions, and the problem were solved using an incremental solution algorithm that solves the thermal and structural responses alternately, the effect could be better simulated.

Conclusions and Recommendations

Failure is likely to occur in the top and side brackets if the leading edge assembly is rigidly constrained as modeled. The FEA results for the top and side brackets are somewhat conservative since some slipping will occur between the bolt and the sting flange. However, slipping is also undesirable since the displaced brackets will remain displaced upon cooldown.

Stress in the top bracket's large bend radius (L1) approaches the failure limit. It is strongly recommended to modify the sting attachment scheme by designing in more compliance to alleviate stress formed in the L1 region. One design possibility is to restrain the top brackets in the z direction with a high temperature spring attached to the right and left top brackets instead of rigidly bolting them to the sting. When the side brackets begins to expand, the top brackets will slide outward in the slot formed by the two halves of the side brackets and will be tensioned such that, upon cooling, the top brackets will be forced back into their original position.

Even though the maximum tip temperature is below the single use limit, failure may occur in the tip insert because large tensile stresses in the z direction approach the failure stress of the material. These stresses may be mitigated by shortening the dovetail of the tip insert. This result maybe conservative as well, however, because the insulating effect of the oxide layer is not taken into account.

References

1. Bull, J. D. et al.: Material Response of Diboride Matrix Composites to Low Pressure Simulated Hypersonic Flows. NASA CP-3235, Part 2, May 1994, pp. 653–673.
2. Buesking, K. W.; Shehan, J. E.; and Sullivan, B. J.: C/HfC Composite for Reentry Vehicle Leading Edges. NSWC Contract Technical Report No. N60921-93-C-0161, Oct. 1994.
3. Glynn, M.; and Buesking, K.W.: Analysis and Design of a Ceramic Matrix Composite Test Fixture for an Advanced Airframe Leading Edge. NASA ARC Contract Report for P.O. A45540D.
4. Hypervelocity Missile Concept Definition Report. LA-CP-94221.
5. Kolodziej, P.: Steady State Aerothermal Performance Constraints for Sharp Leading Edges of Hypersonic Vehicles. To be published as a NASA TM.
6. Lees, L.: Laminar Heat Transfer Over Blunt-Nosed Bodies at Hypersonic Flight Speeds. Jet Propulsion, vol. 26, no. 4, Apr. 1956, pp. 259–269.
7. Marvin, J. G.; and Deiwert, G. S.: Convective Heat Transfer in Planetary Gases. NASA TR-224, Feb. 1965.

Appendix

```
C*File: s2mbeta.txt 10/95
C*This script maps heat teansfer coefficients (as a function of S/R)
C*to finite elements of an extruded leading edge model created with
C*COSMOS/M.  The heat transfer coefficient/S/R curves repesent
C*conditions for vehicle re-entry at an altitude of 60 km and were
C*determined by iteratively solving a 2d profile Heat transfer model
C*in conjuction with ACE code. (ref. Paul Koldijiez)
C*
C*Tom Kowalski, Eloret
C*Thermal protection Materials and Systems Branch (STM)
C*NASA Ames Research Center.
C*9/14/95
C*
C*NOTE: O,O,O IS AT THE RIGHT MOST RADIAL CENTER
C*
C*Function definitions for hcoef and s/r
C*PARASSIGN, A1, REAL, -9.0911925
C*PARASSIGN, B1, REAL, -1.004798
C*PARASSIGN, C1, REAL, 9.040512
C*PARASSIGN, D1, REAL, .37909244
C*PARASSIGN, E1, REAL, -3.613106
C*PARASSIGN, A2, REAL, 6.4622922E-5
C*PARASSIGN, B2, REAL, -3.56788E-5
C*PARASSIGN, C2, REAL, -2.3938027E-5
C*PARASSIGN, D2, REAL, 8.1591626E-6
C*PARASSIGN, E2, REAL, 5.618041E-6
C*PARASSIGN, F2, REAL, 6.7637685E-7
C*
FUNCDEF, HTCO2(X1), REAL, EXP((-9.0911925&
+9.040512*X1-3.613106*X1^2)/(1-1.004798*X1+&
.37909244*X1^2))
FUNCDEF, HTC270(X2), REAL, (6.4622922E-5)&
-((3.56788E-5)*LOG(X2))-((2.3938027E-5)/LOG(X2))+&
((8.1591626E-6)*(LOG(X2))^2)+&
((5.618041E-6)/(LOG(X2))^2)-((6.7637685E-7)*(LOG(X2))^3)
C*
PARASSIGN, LENGTH, REAL,6.80
PARASSIGN, ALPHA, REAL, (5*PI/180)
PARASSIGN, RAD, REAL,.11
PARASSIGN, MINESZ, REAL, .0145
PARASSIGN, STRLINE, REAL, (LENGTH-RAD+RAD*SIN(ALPHA))/COS(ALPHA)
PARASSIGN, STRARC, REAL, RAD*((PI/2)-ALPHA)
PARASSIGN, STRTOT, REAL, (STRLINE+STRARC)
PARASSIGN, TSTRSTPS, REAL, CEIL(STRTOT/MINESZ)
PARASSIGN, STRIN, REAL, 1
PARASSIGN, TZSTPS1, REAL, 4
PARASSIGN, ZSTPSZ1, REAL, .2175
PARASSIGN, ZSTART1, REAL, 0
PARASSIGN, TZSTPS2, REAL, 6
PARASSIGN, ZSTPSZ2, REAL, .33416
PARASSIGN, ZSTART2, REAL, .87
PARASSIGN, ZLOC, REAL, ZSTPSZ1
```

```
C*Face numbering issue
C* Assign location along streamiline at the end of the first
C*set of brick elements
PARASSIGN, ebrkset1, REAL, .19053
PARASSIGN, sbrkset2, REAL, .22563
INITSEL, EL, 1, 0;
INITSEL, ND, 1, 0;
ACTSET, CS, 19;
C*
C*#LOOP LABEL10 TZSTPS1
C*#LOOP LABEL20 TSTRSTPS
#LOOP LABEL20 10
PARASSIGN, STRLOC1, REAL,STRIN*MINESZ
PARASSIGN, SR, REAL, STRLOC1/RAD
#IF (SR>0) && (SR<=2)
PARASSIGN, HTC, REAL, HTCO2(SR)
PARASSIGN, TAMB, REAL, 47510
#ELSE
PARASSIGN, HTC, REAL, HTC270(SR)
PARASSIGN, TAMB, REAL, 47400
#ENDIF
#IF (STRLOC1>0) && (STRLOC1<=STRARC)
PARASSIGN, XLOC, REAL, RAD*COS(SR)
PARASSIGN, YLOC, REAL, RAD*SIN(SR)
#ELSEIF (STRLOC1>STRARC) && (STRLOC1<=.22176)
PARASSIGN, XLOC, REAL, STRLOC1*COS(ALPHA)-RAD*SIN(ALPHA)
PARASSIGN, YLOC, REAL, RAD*COS(ALPHA)+STRLOC1*SIN(ALPHA)
#ELSE
PARASSIGN, XLOC, REAL, STRLOC1*COS(ALPHA)-RAD*SIN(ALPHA)
PARASSIGN, YLOC, REAL, .040+(RAD*COS(ALPHA)+STRLOC1*SIN(ALPHA))
#ENDIF
PARASSIGN, LOCNOD, INT, NEARND(XLOC|YLOC|ZLOC)
INITSEL, EL;
SELREF,EL,ND,LOCNOD,LOCNOD,1;
#IF (STRLOC1>0) && (STRLOC1<=ebrkset1)
C* FIRST SET OF BRICK ELEMENTS ON CURVED SECTION, FACE 4 C*EXPOSED
CEL, 1,HTC, TAMB,2,ELMAX,1,0
#ELSEIF (STRLOC1>ebrkset1) && (STRLOC1<=.22176)
C* SECOND SET OF BRICK ELEMENTS, FACE 3 EXPOSED
CEL, 1,HTC, TAMB,3,ELMAX,1,0
#ELSE
C*SHELL ELEMENTS, FACE 5 EXPOSED
CEL, 1,HTC, TAMB,5,ELMAX,1,0
#ENDIF
INITSEL, EL;
PARASSIGN, STRIN, INT, STRIN+1
#LABEL LABEL20
C*PARASSIGN, REAL, ZLOC, ZLOC+ZSTPSZ1
C*#LABEL LABEL10
```

Table 1(a). Computed mechanical properties for 35 vol.% SCS-9a-[RBSiC/ZrB_2] unidirectional laminate

Temp (°F)	E_0 (msi)	E_{90} (msi)	ν_{0-90}	G_{0-90} (msi)	σ_0^{tens} (ksi)	σ_0^{comp} (ksi)	σ_{90}^{tens} (ksi)	σ_{90}^{comp} (ksi)	τ (ksi)
75	20.74	12.24	0.140	5.58	77.4	154.7	4.9	4.3	2.8
1000	20.42	13.63	0.136	6.19	97.0	193.9	6.7	4.3	3.9
2000	19.29	12.80	0.136	5.81	75.6	151.2	8.2	4.3	4.7
3000	18.91	17.01	0.136	7.57	54.3	108.5	8.6	4.3	5.0

Table 1(b). Thermal properties for 35 vol.% SCS-9a-[RBSiC/ZrB_2] unidirectional laminate

Temp (°F)	α_0 (10^{-6}/°F)	α_{90} (10^{-6}/°F)	K_x (Btu/in.-s-F × 10^3)	K_y (Btu/in.-s-F × 10^3)
75	3.29	3.71	3.65	2.70
1000	3.34	3.71	1.60	1.30
2000	3.34	3.71	0.94	0.63
3000	3.54	3.73	0.74	0.39

Table 2. Contact forces between top and side brackets

Element	F_x (Lbf)	F_y (Lbf)	F_z (Lbf)	Gap dist. (in)	Normal force (Lbf)
1093	0.00	0.00	3.81	0.00	3.81
1128	0.00	–1.29	0.00	0.00	1.29
1137	0.00	–0.85	0.00	0.00	0.85
1242	0.00	0.00	148.30	0.00	148.30
1243	0.00	0.00	230.60	0.00	230.60
Total	0.00	–2.14	382.70		

Table 3. Locations of concern identified in thermostructural analysis of UHTC protoype leading edge assembly

Component	Location	Concern	Cause(s)	Recommendations
Top bracket	Bend radius L1	*Significant.* Failure index approaches 1.0	Contact via thermal growth of side bracket	a) Retrofit with slider and spring return mechanism (fig 19) b) Trim side bracket
	Sharp corner junction L2	*Low.* Result is conservative. Actual geometry is rounded here.	a) Thermal growth of side bracket b) Thermal growth of tip insert	None
	Bolted region L3	*Moderate.* Result is slightly conservative. In reality bracket will slide under bolt preload.	a) Thermal growth of top bracket (300°F) b) Contact via thermal growth of side bracket c) Design constraints (real and imposed)	a) Retrofit with slider and spring return mechanism (fig 19) b) Trim side bracket c) If bolt is used, install with graphite washer, to reduce static friction between bearing surfaces Note: Solution "c" offers no return mechanism.
Side bracket	Bolted region L4	*Moderate.* Result is conservative. In reality bracket will slide under bolt preload.	a) Reaction force via contact with top bracket (383 lbf in Z) due to thermal growth of side bracket b) Thermal growth of side bracket (300°F)	a) Retrofit with slider and spring return mechanism (fig 19) a) Design more compliance in to fastening scheme for side bracket. graphite washers, etc.
	Center L6	*Moderate*	a) Temperature difference of fore and aft section	None
Tip insert	Tip center at peak temperature L5	*Low.* Compressive stress 250 ksi, half of compressive strength	Temperature difference between tip and dovetail. Hot material expands, but growth is restricted by neighboring cooler material which places hot material in compression.	None. Safety factor: 2

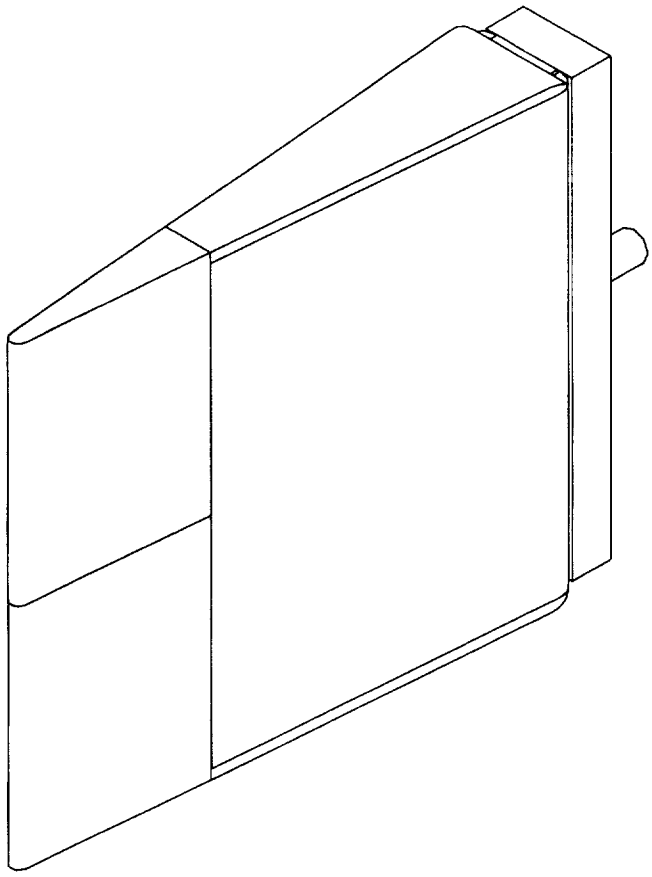

Figure 1. Prototype leading edge assembly.

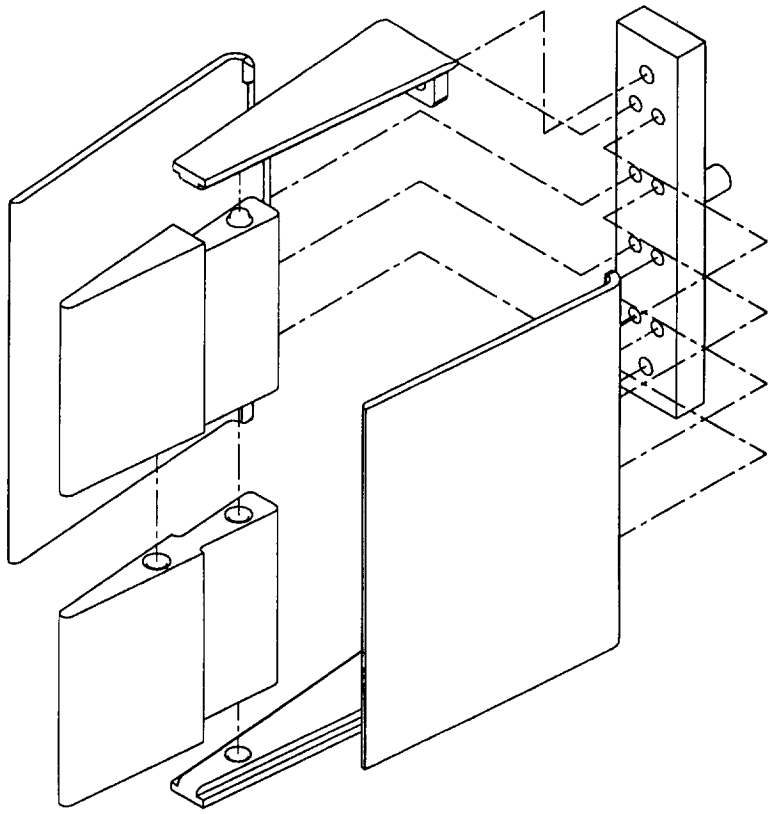

Figure 2. Exploded view of leading edge assembly.

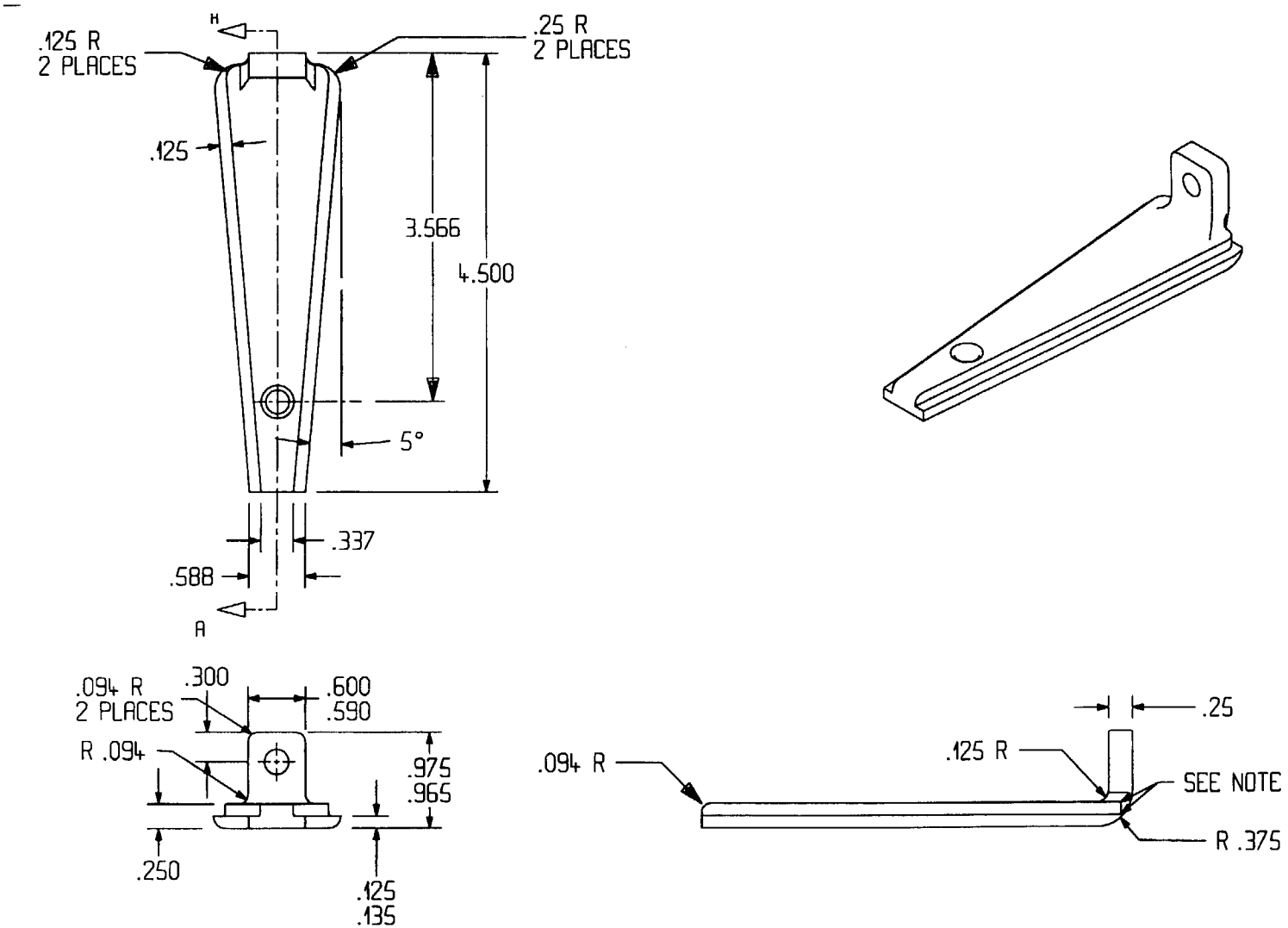

Figure 3. Top bracket geometry.

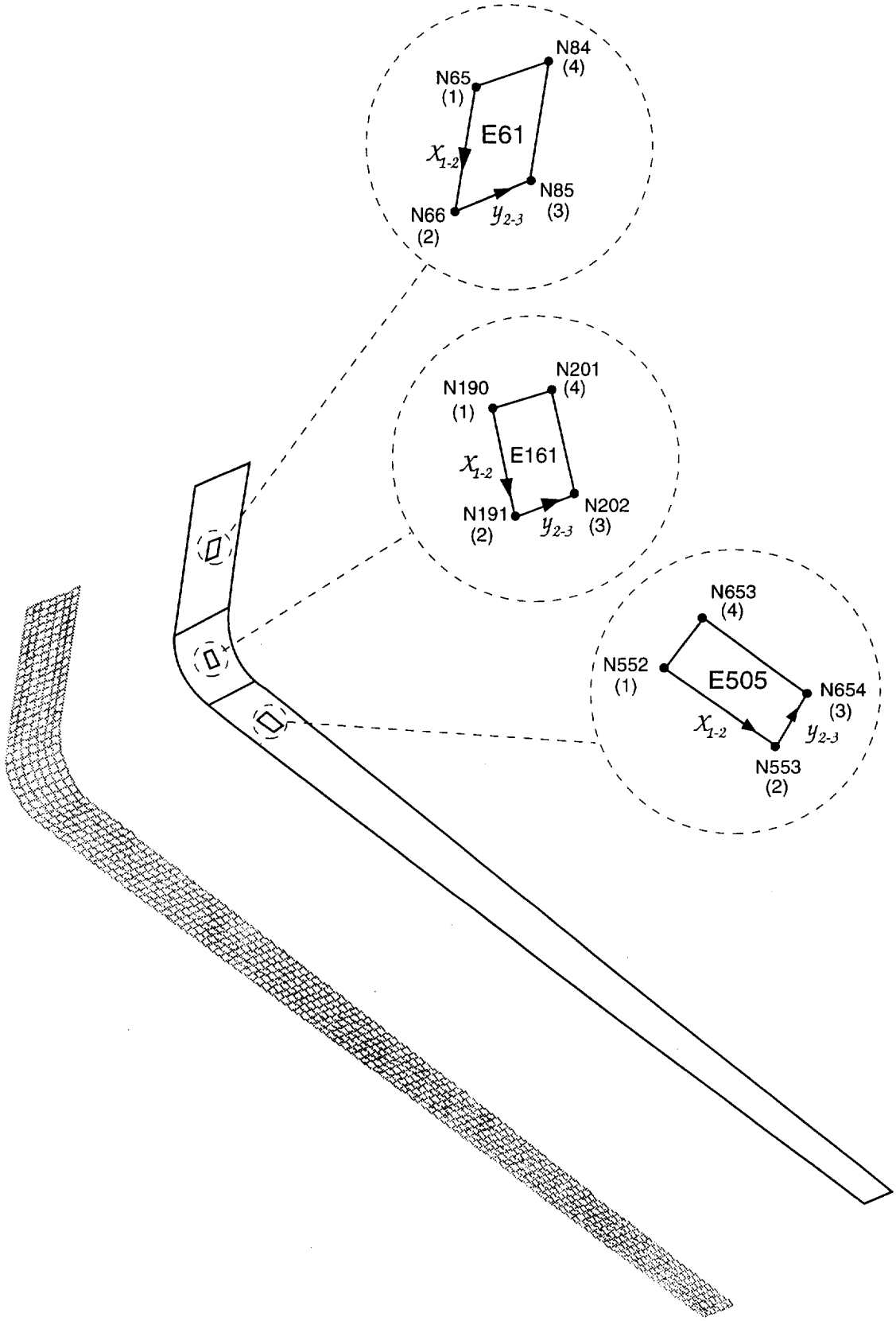

Figure 4. Cosmos top bracket mesh with element coordinate system definition.

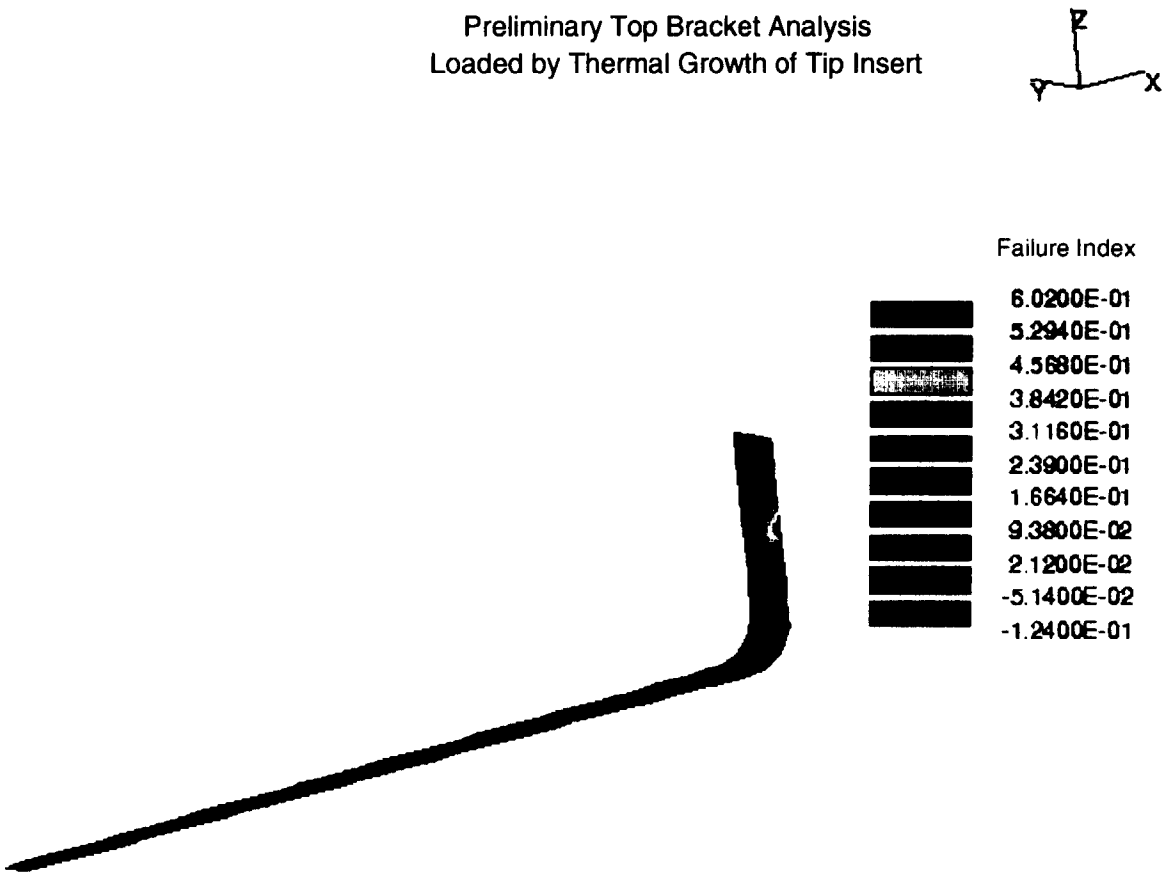

Figure 5. COSTAR solution, Tsai-Wu failure index for ply 1 of top bracket (0/90).

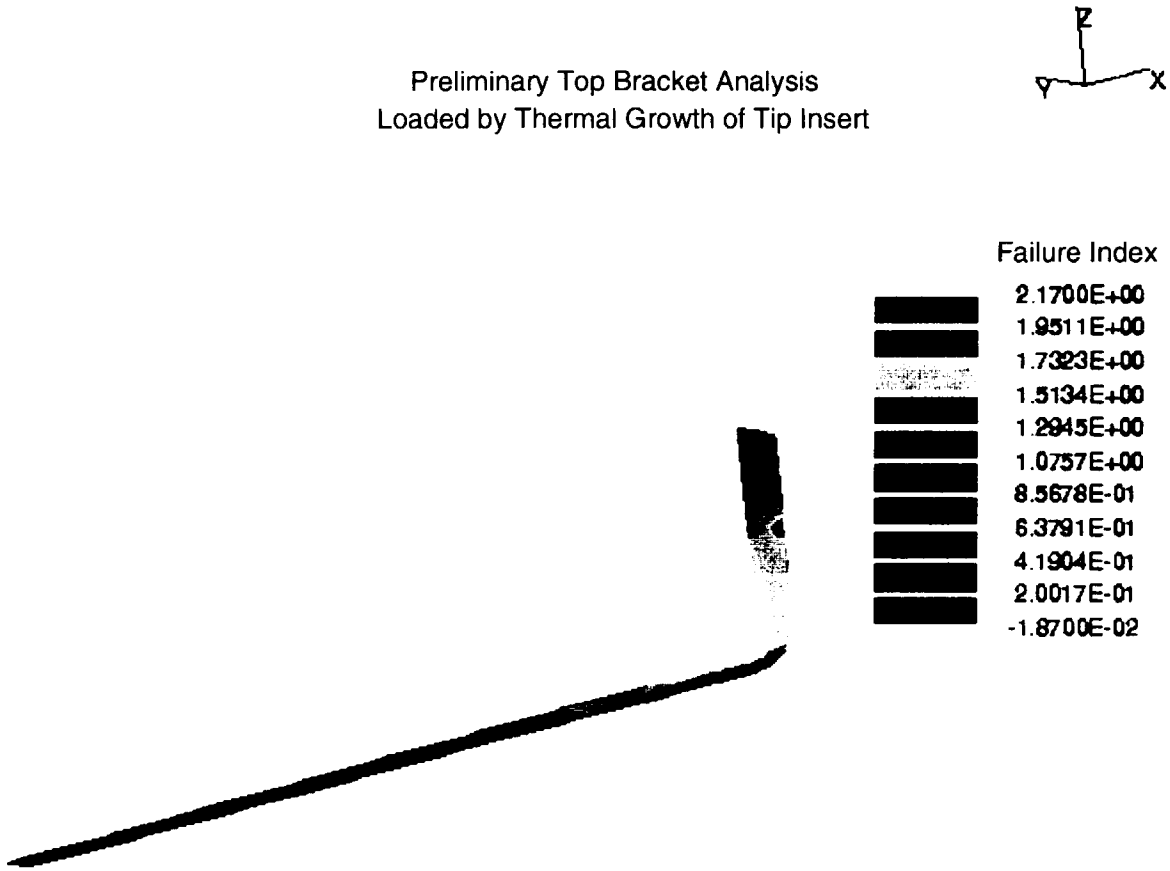

Figure 6. COSTAR solution, Tsai-Wu failure index for ply 2 of top bracket (0/90).

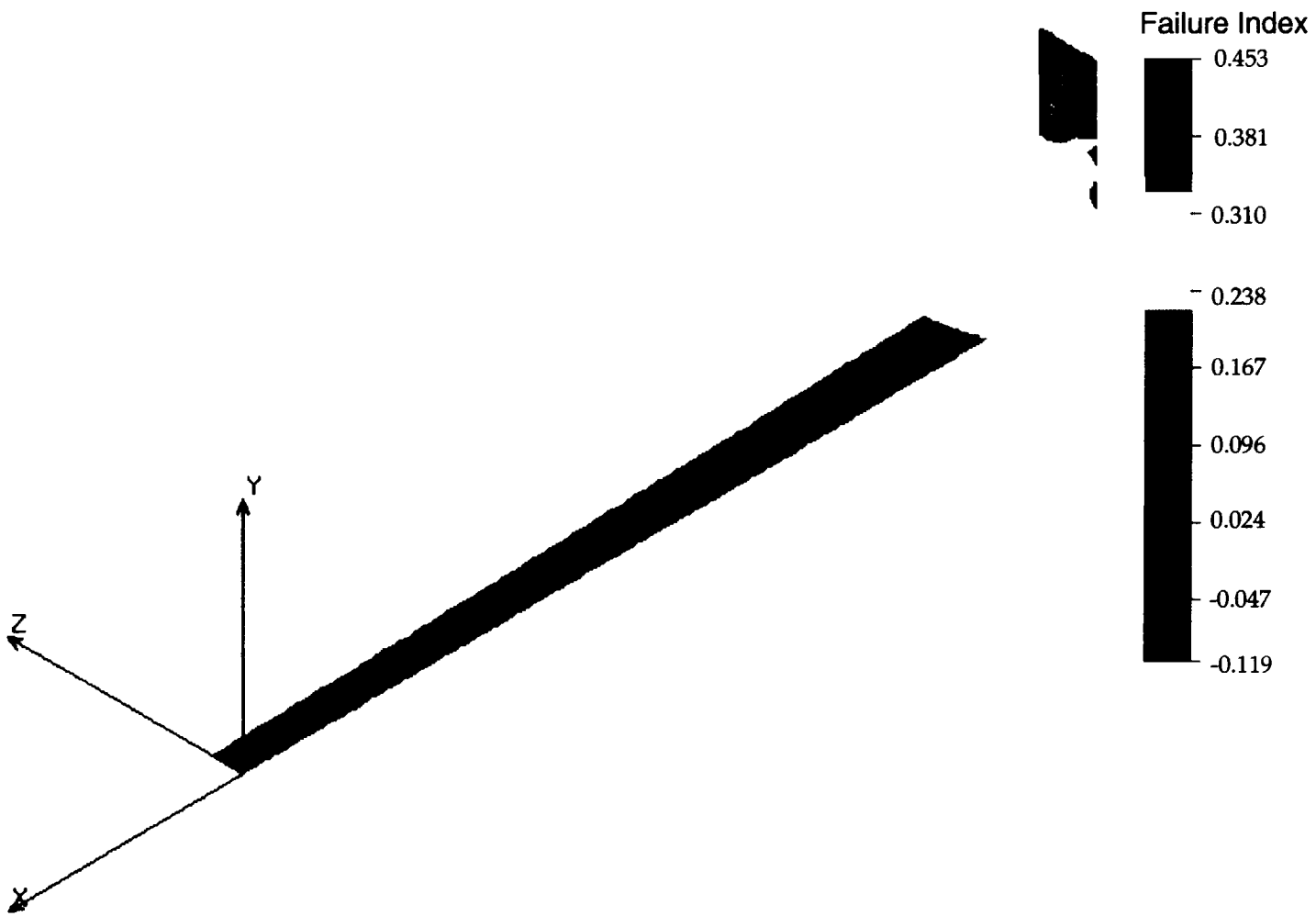

Figure 7. COSMOS solution, Tsai-Wu failure index for ply 1 of top bracket (0/90).

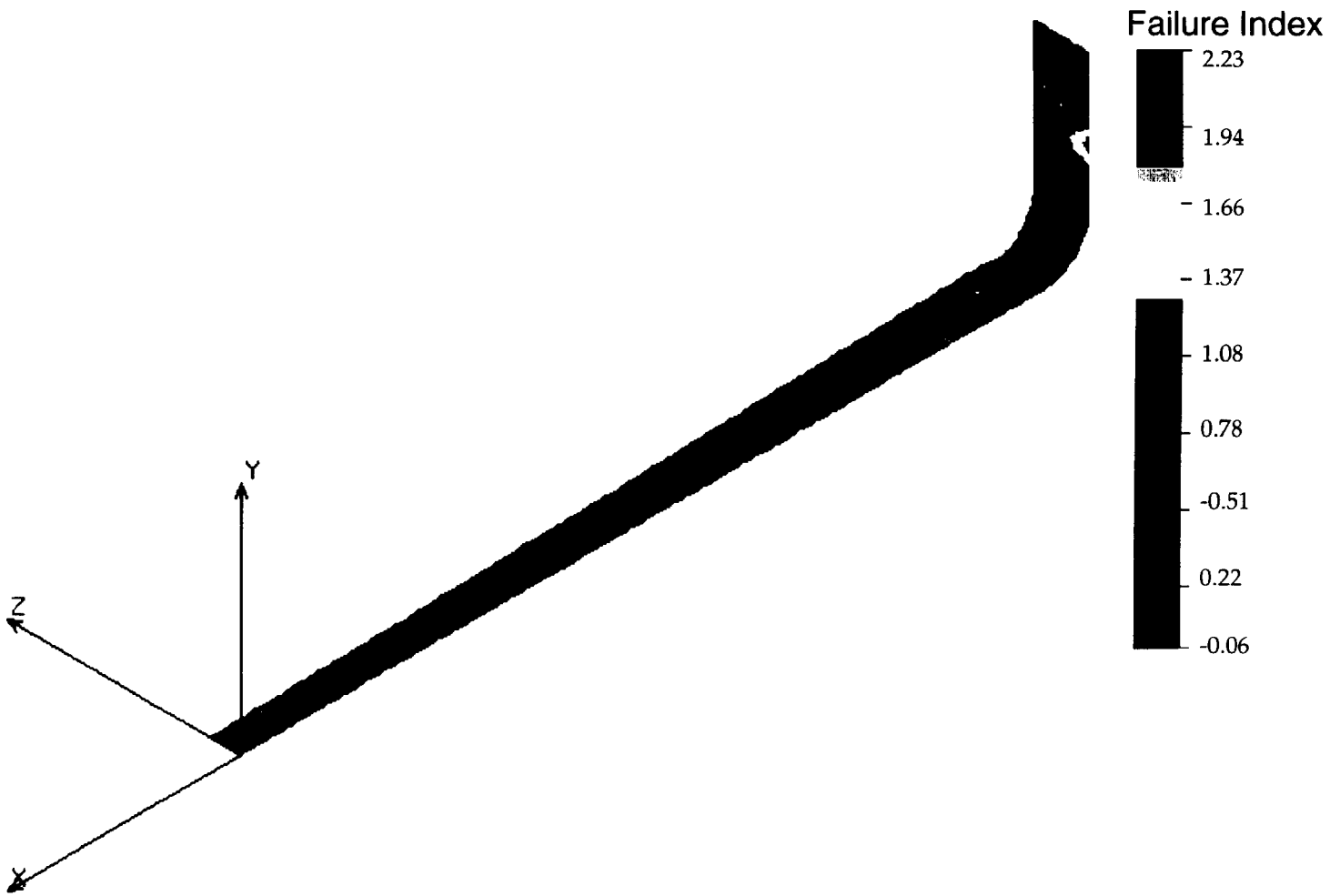

Figure 8. COSMOS solution, Tsai-Wu failure index for ply 2 of top bracket (0/90).

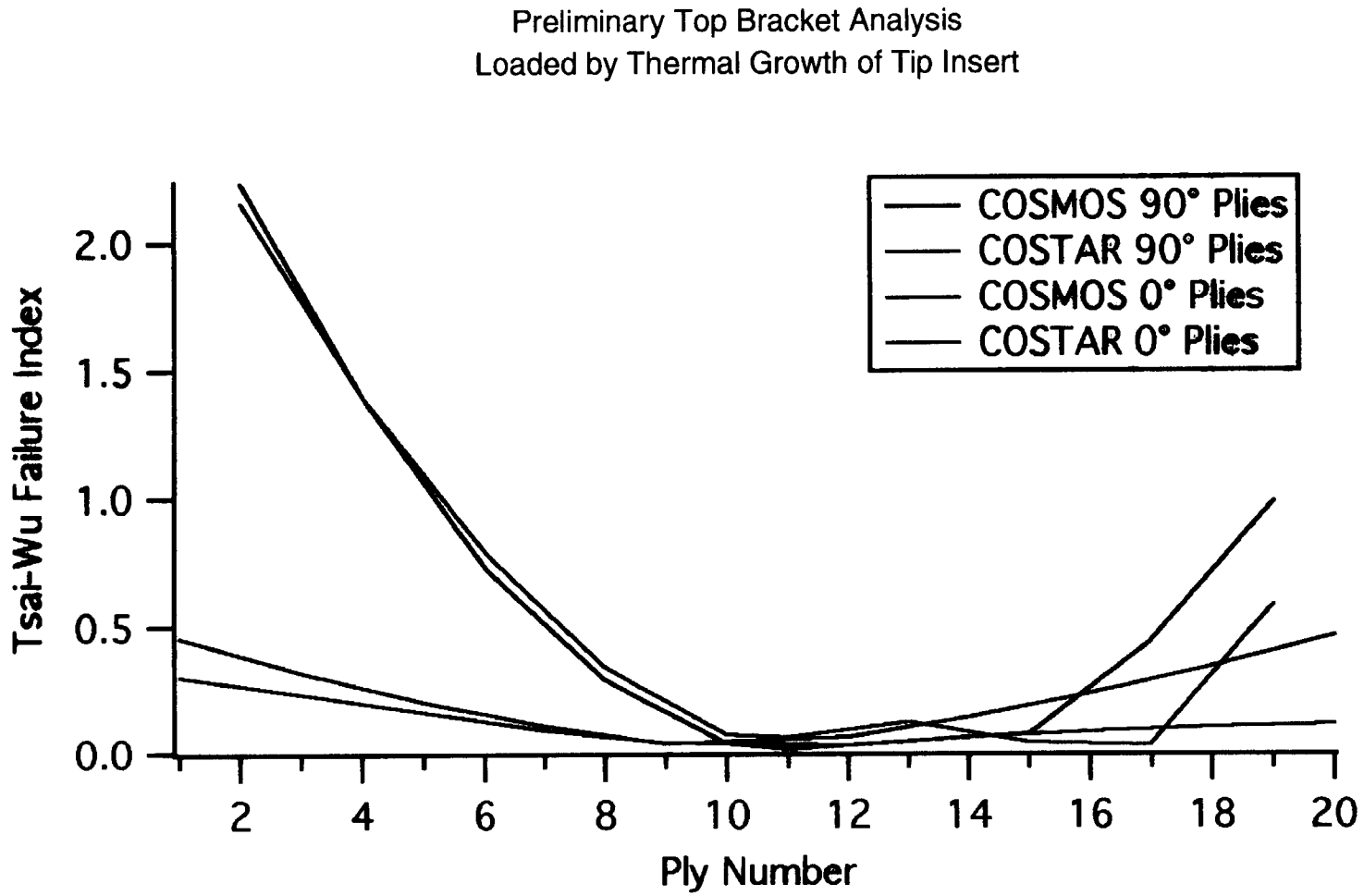

Figure 9. Through thickness failure index comparison for 0/90 lay-up.

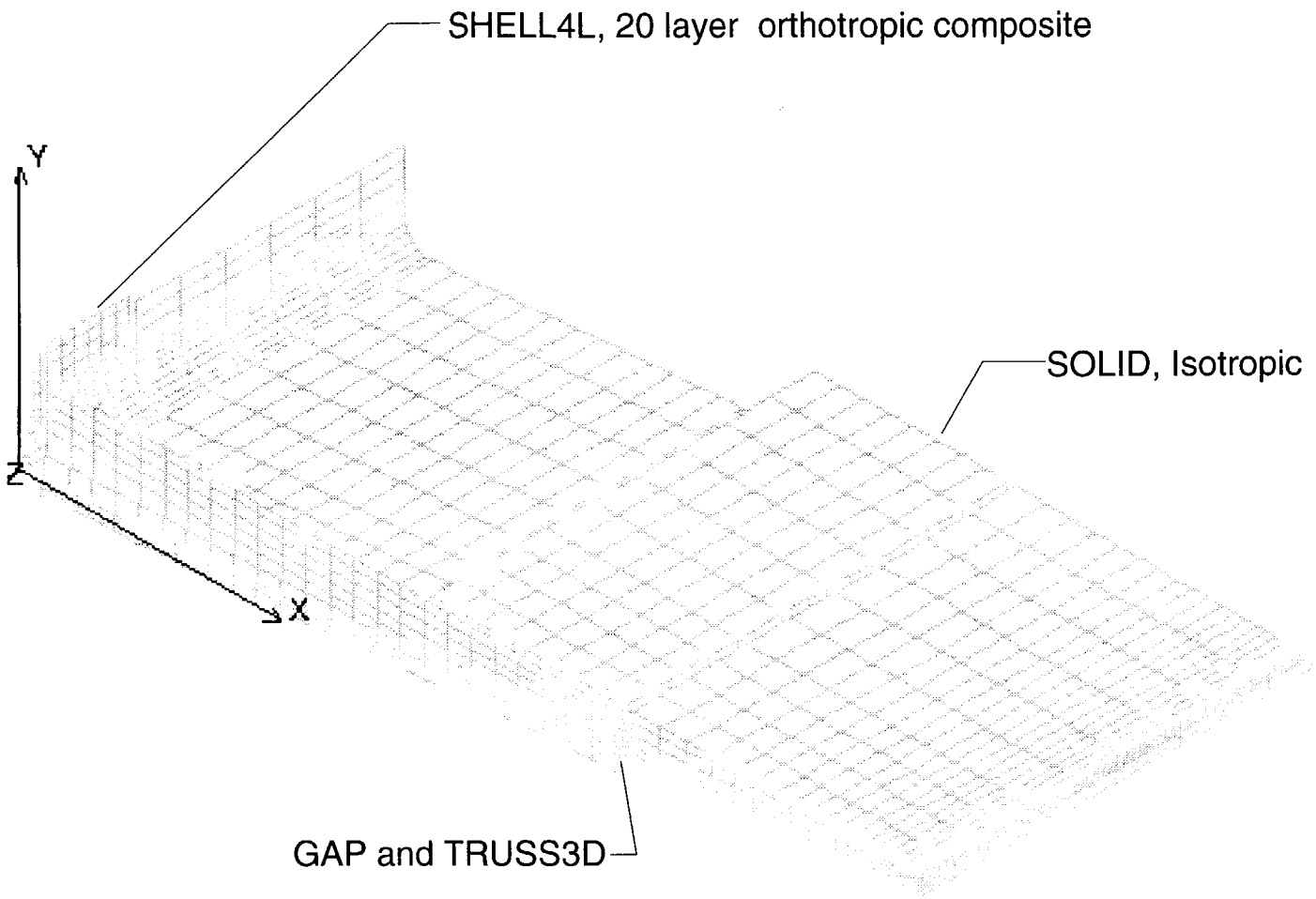

Figure 10. Element plot of finite element model for leading edge assembly.

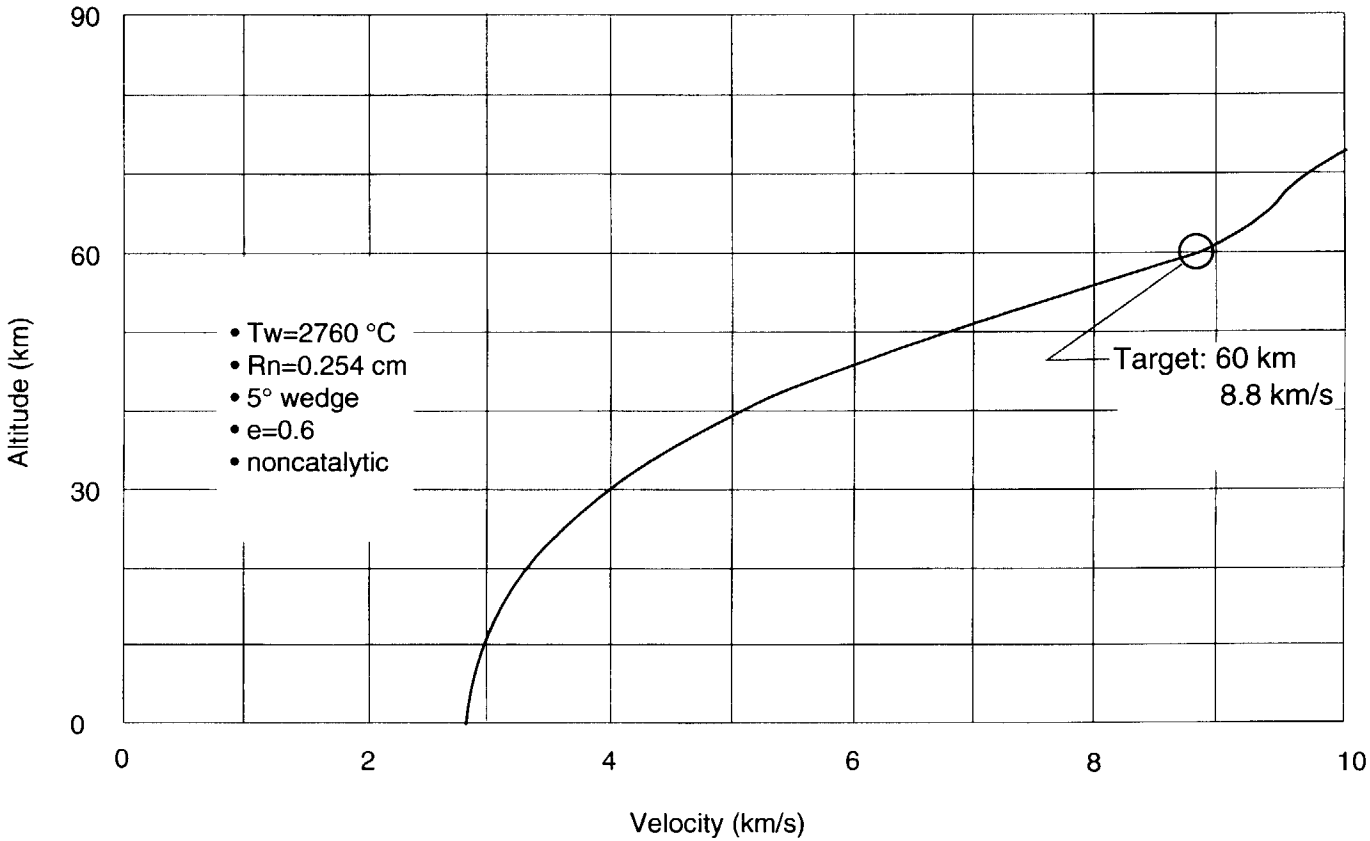

Figure 11(a). Steady state aerothermal performance constraint for diboride composite.

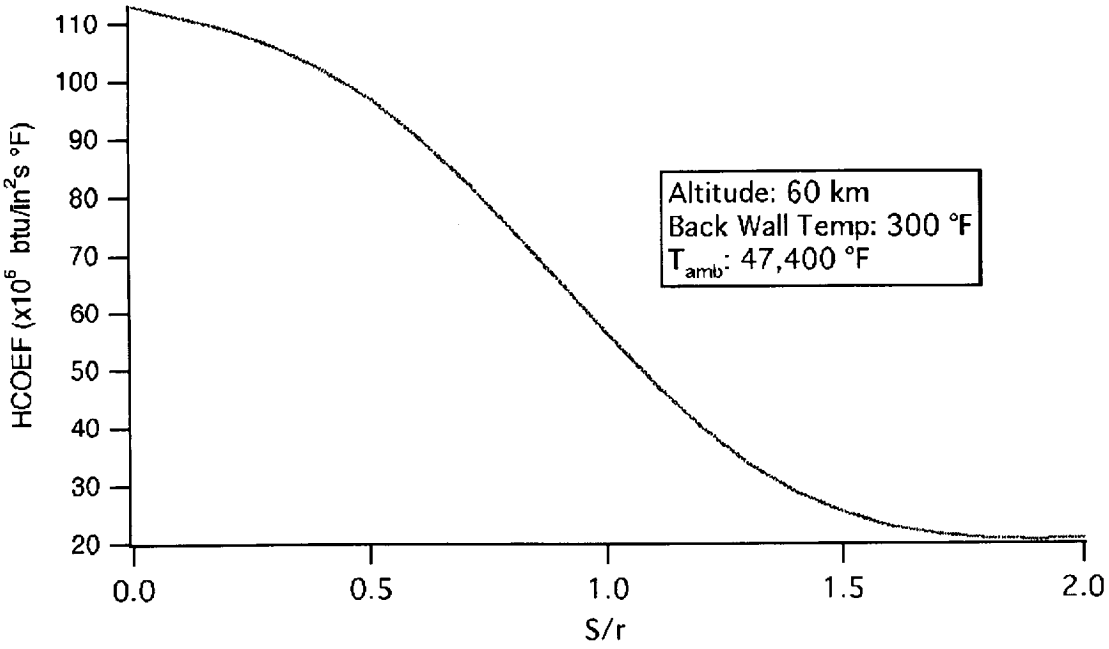

Figure 11(b). Convective heat transfer coefficient vs. S/r at target point indicated in figure 11(a) (range: 0 < S/r < 2).

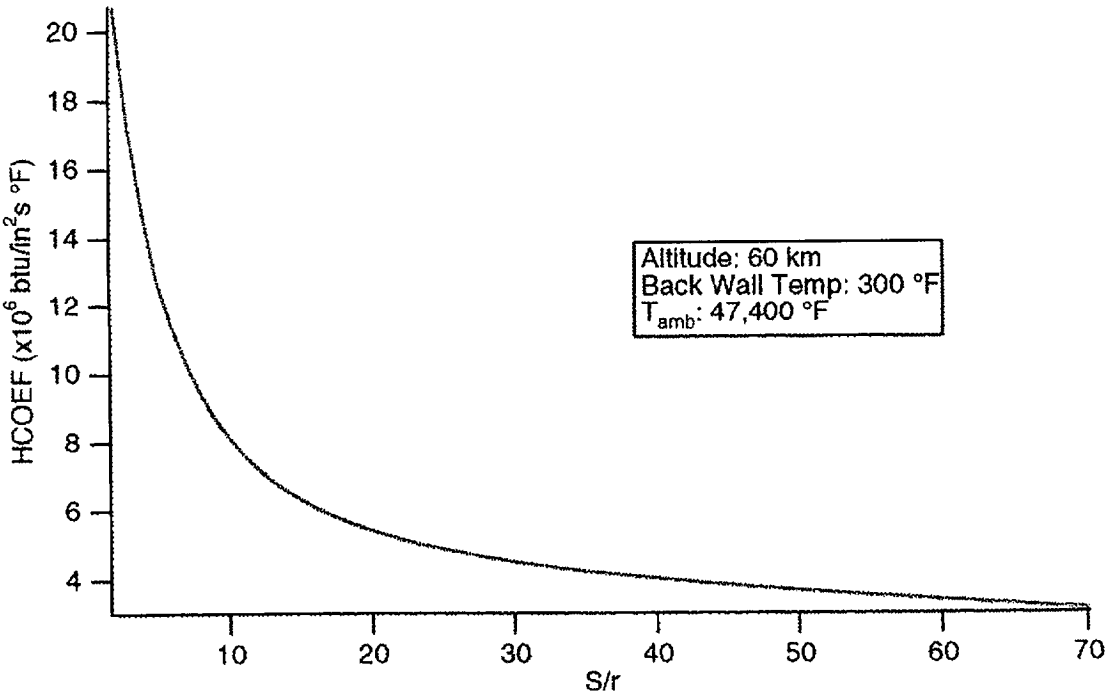

Figure 11(c). Convective heat transfer coefficient vs. S/r at target point indicated in figure 11(a) (range: 2 < S/r < 70).

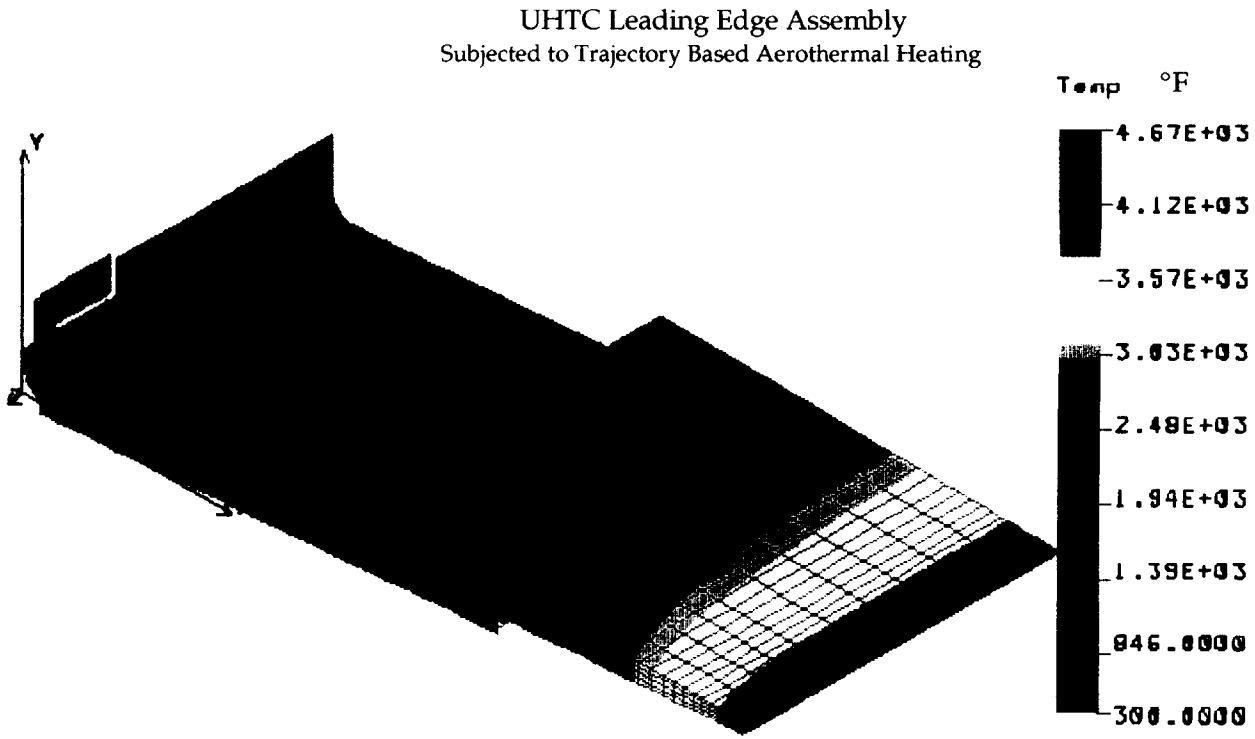

Figure 12. Top-side view of steady state temperature distribution plot.

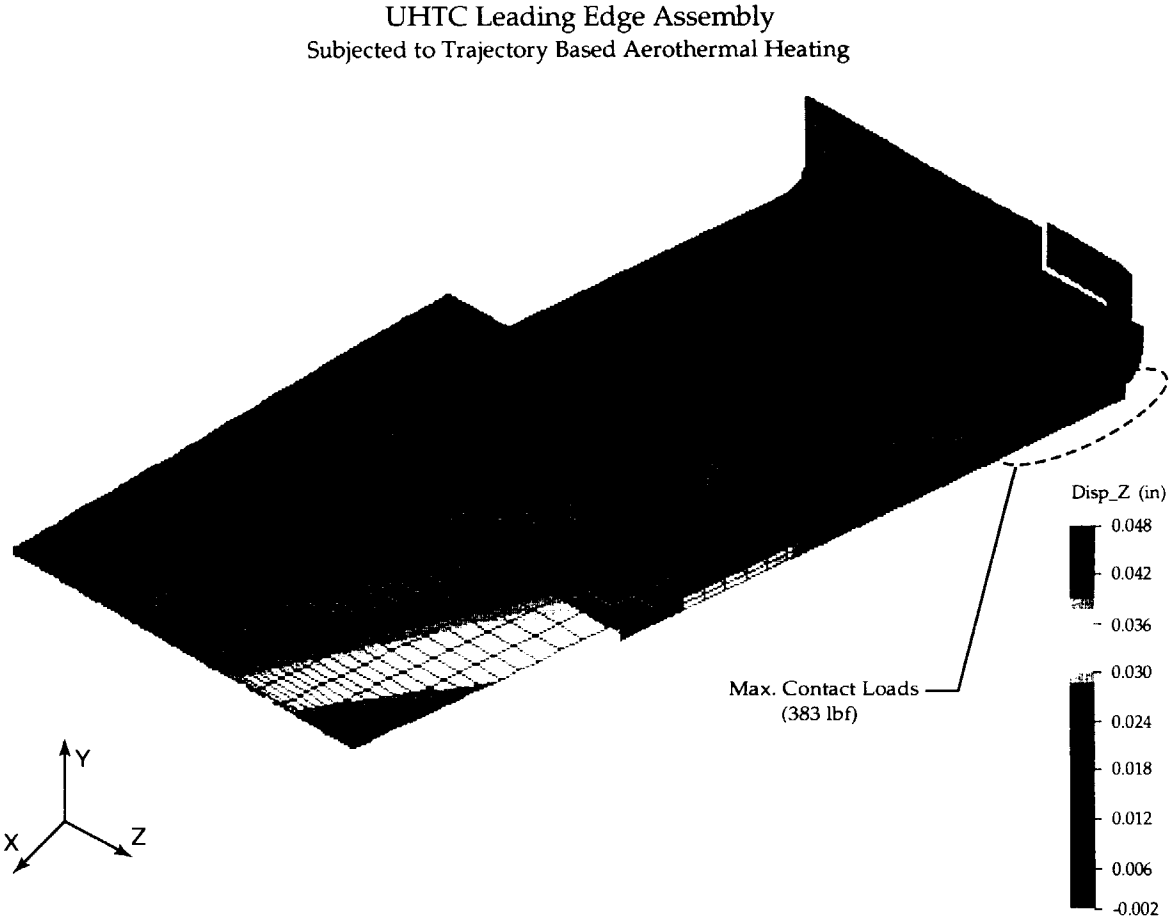

Figure 13. Underside view of displacement plot.

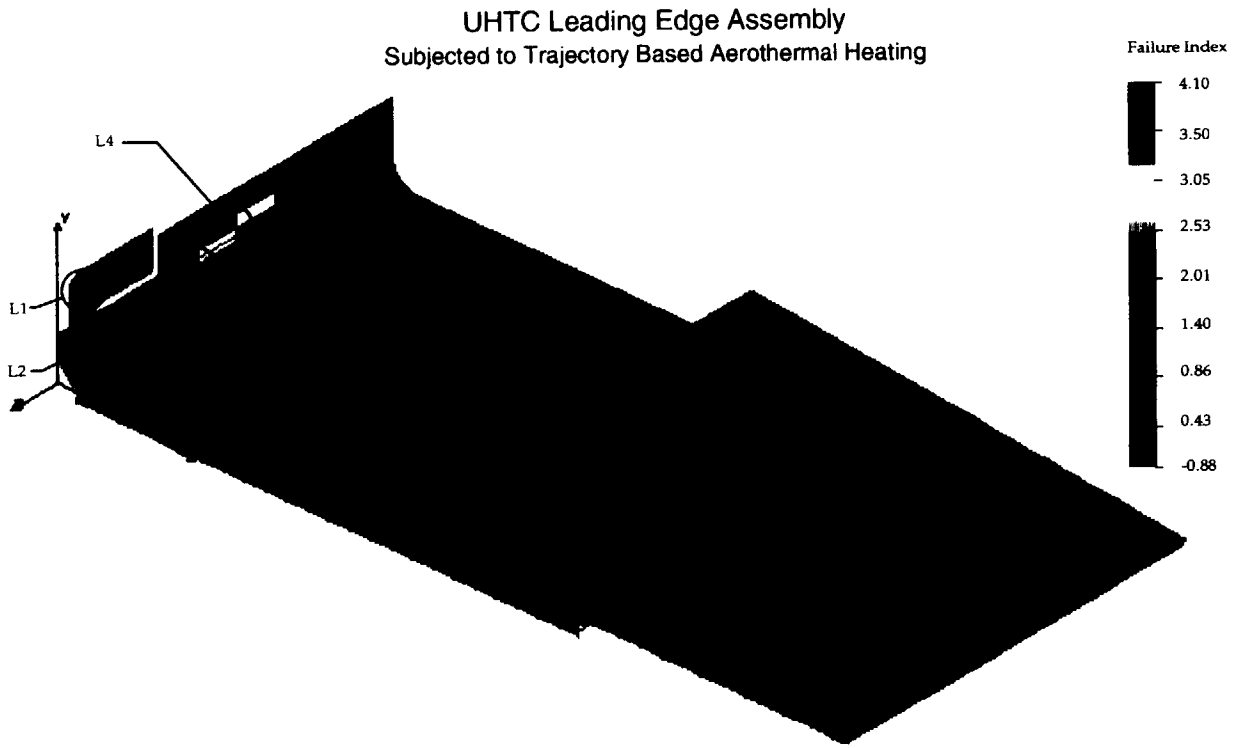

Figure 14. Tsai-Wu failure index plot—ply 2.

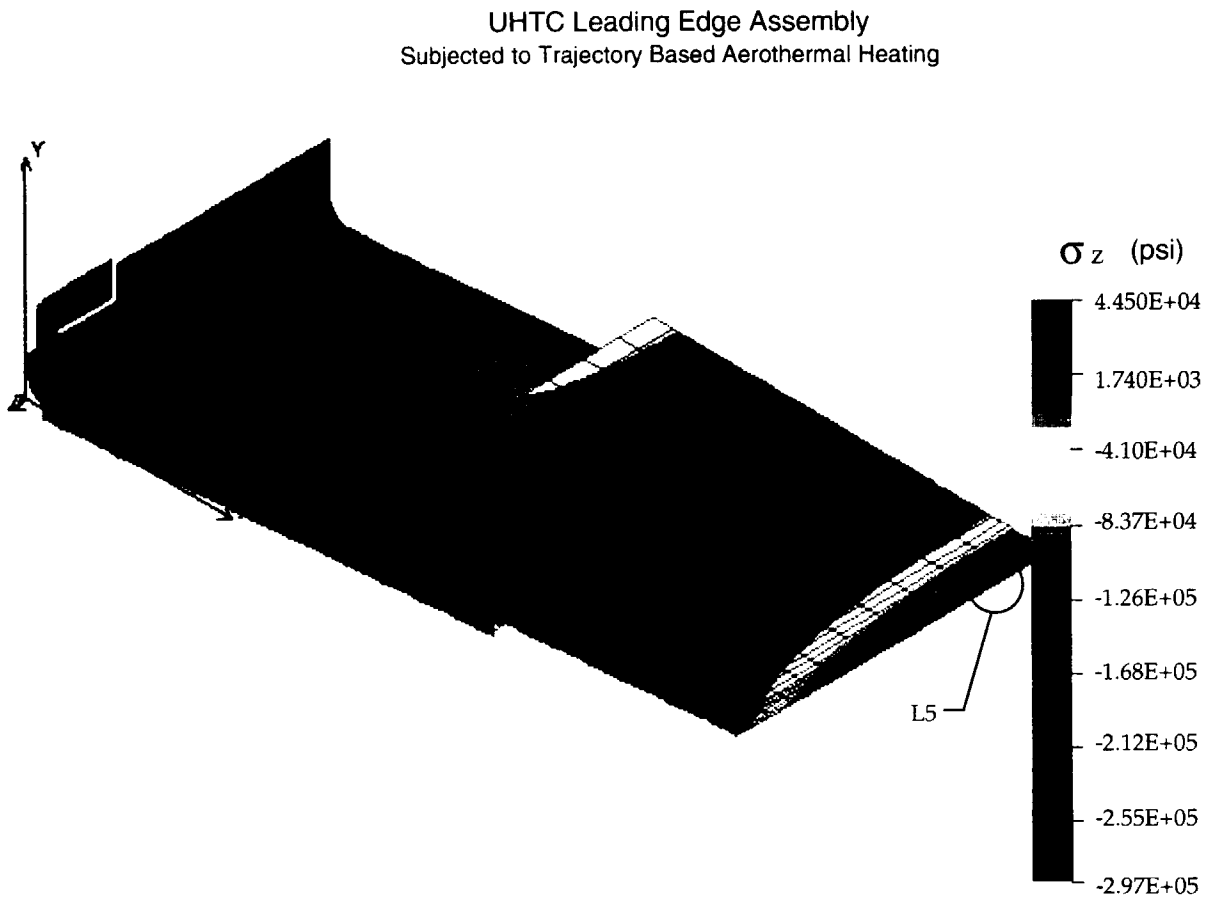

Figure 15. Stress plot in the z-direction—ply 1.

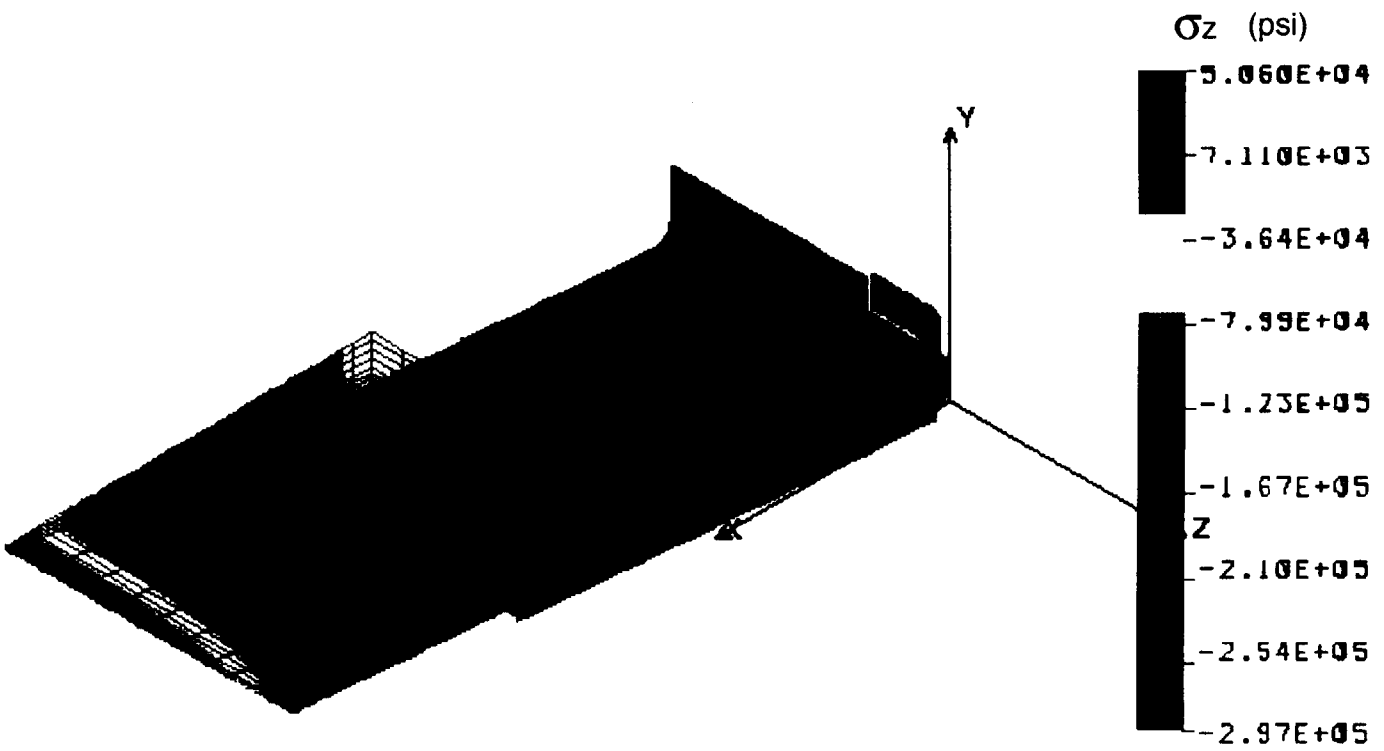

Figure 16. Stress plot in the z-direction—ply 2.

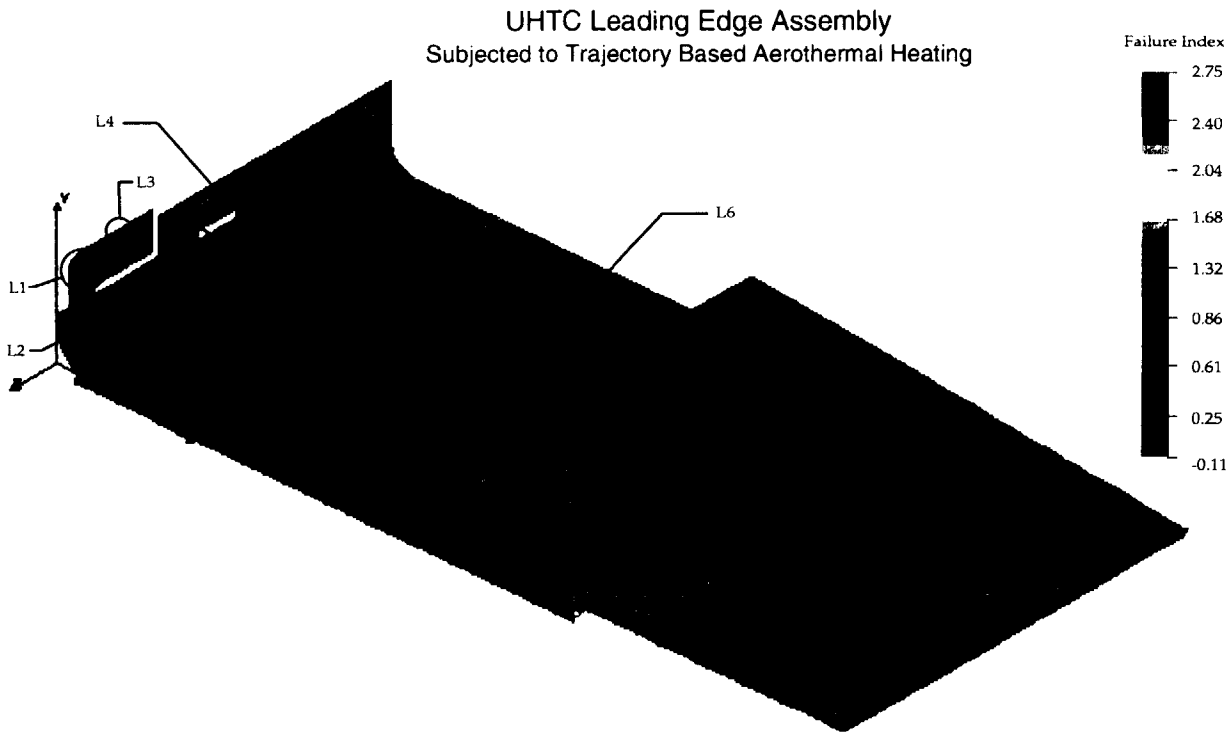

Figure 17. Tsai-Wu failure index plot—ply 1.

REPORT DOCUMENTATION PAGE

Form Approved
OMB No. 0704-0188

Public reporting burden for this collection of information is estimated to average 1 hour per response, including the time for reviewing instructions, searching existing data sources, gathering and maintaining the data needed, and completing and reviewing the collection of information. Send comments regarding this burden estimate or any other aspect of this collection of information, including suggestions for reducing this burden, to Washington Headquarters Services, Directorate for information Operations and Reports, 1215 Jefferson Davis Highway, Suite 1204, Arlington, VA 22202-4302, and to the Office of Management and Budget, Paperwork Reduction Project (0704-0188), Washington, DC 20503.

1. AGENCY USE ONLY *(Leave blank)*	2. REPORT DATE	3. REPORT TYPE AND DATES COVERED
	July 1996	Technical Memorandum

4. TITLE AND SUBTITLE

A Thermostructural Analysis of a Diboride Composite Leading Edge

5. FUNDING NUMBERS

242-80-01

6. AUTHOR(S)

Tom Kowalski,* Kent Buesking,† Paul Kolodziej, and Jeff Bull

7. PERFORMING ORGANIZATION NAME(S) AND ADDRESS(ES)

Ames Research Center
Moffett Field, CA 94035-1000

8. PERFORMING ORGANIZATION REPORT NUMBER

A-962040

9. SPONSORING/MONITORING AGENCY NAME(S) AND ADDRESS(ES)

National Aeronautics and Space Administration
Washington, DC 20546-0001

10. SPONSORING/MONITORING AGENCY REPORT NUMBER

NASA TM-110407

11. SUPPLEMENTARY NOTES

Point of Contact: Jeff Bull, Ames Research Center, MS 234-1, Moffett Field, CA 94035-1000
(415) 604-5377
*Eloret Thermosciences Institute, Palo Alto, California. †MSNW, Inc., San Marcos, California.

12a. DISTRIBUTION/AVAILABILITY STATEMENT

Unclassified — Unlimited
Subject Category 39

12b. DISTRIBUTION CODE

13. ABSTRACT ***(Maximum 200 words)***

In an effort to support the design of zirconium diboride composite leading edges for hypersonic vehicles, a finite element model (FEM) of a prototype leading edge was created and finite element analysis (FEA) was employed to assess its thermal and structural response to aerothermal boundary conditions. Unidirectional material properties for the structural components of the leading edge, a continuous fiber reinforced diboride composite, were computed with COSTAR. These properties agree well with those experimentally measured. To verify the analytical approach taken with COSMOS/M, an independent FEA of one of the leading edge assembly components was also done with COSTAR. Good agreement was obtained between the two codes. Both showed that a unidirectional lay-up had the best margin of safety for a simple loading case. Both located the maximum stress in the same region and ply. The magnitudes agreed within 4 percent. Trajectory based aerothermal heating was then applied to the leading edge assembly FEM created with COSMOS/M to determine steady state temperature response, displacement, stresses, and contact forces due to thermal expansion and thermal strains. Results show that the leading edge stagnation line temperature reached 4700°F. The maximum computed failure index for the laminated composite components peaks at 4.2, and is located at the bolt flange in layer 2 of the side bracket. The temperature gradient in the tip causes a compressive stress of 279 ksi along its width and substantial tensile stresses within its depth.

14. SUBJECT TERMS	15. NUMBER OF PAGES
Diboride composite, Thermostructural analysis, Finite element analysis	32
	16. PRICE CODE: A03

17. SECURITY CLASSIFICATION OF REPORT	18. SECURITY CLASSIFICATION OF THIS PAGE	19. SECURITY CLASSIFICATION OF ABSTRACT	20. LIMITATION OF ABSTRACT
Unclassified	Unclassified		